

Electric Double Layer from Phase Demixing Reinforced by Strong Coupling Electrostatics

YeongKyu Lee* and YongSeok Jho†
Physics Department, Gyeongsang National University

JunBeom Cho,* Yongkyu Lee, and Won Bo Lee‡
School of Chemical and Biological Engineering, Seoul National University
(Dated: January 2, 2024)

Ionic liquids (ILs) are appealing electrolytes for their favorable physicochemical properties. However, despite their longstanding use, understanding the capacitive behavior of ILs remains challenging. This is largely due to the formation of a non-conventional electric double layer (EDL) at the electrode-electrolyte interface. This study shows that the short-range Yukawa interactions, representing the large anisotropically charged ILs, demix IL to create a spontaneous surface charge separation, which is reinforced by the strongly coupled charge interaction. The properties of the condensed layer, the onset of charge separation, and the rise of overscreening and crowding critically depend on the asymmetry of Yukawa interactions.

Introduction: Room-temperature ionic liquids (RTILs) are combinations of large organic cations and organic, inorganic anions with delocalized charges. Unlike conventional inorganic salts, these structural characteristics prevent them from forming crystalline structures at room temperature [1–3]. As an electrolyte solvent at ambient conditions, RTILs offer several advantages for energy storage applications, such as low volatility, good solvent properties, high thermal stability, and environmental sustainability [4–9], which are especially fit for future energy storage devices, supercapacitors, or ultracapacitors. Notably, some essential features for high-technology devices (*e.g.* wireless devices and electric cars), such as higher-rate energy harvesting and long-lasting supercapacitance, are related to the electric double layer (EDL) structures in RTILs [10–14]. While conventional point charge models predict the development of a condensation layer at very large surface charge densities, IL exhibits EDL at very low surface charge densities and even overscreening and crowding, which are very difficult to achieve without the presence of the multivalent counterions within the point charge models. The key differences are from the large shape of IL molecules and their delocalized charges. Understanding how to embody these properties in the microscopic mechanism is challenging and crucial in utilizing ILs for energy device applications [15–18].

Bazant, Storey, and Kornyshev (BSK) [19] are among the first to incorporate a short-range electrostatic correlation to the EDL. They showed that a phenomenological modification of the Poisson equation with an extra fourth-order potential gradient term, reflecting a short-range electrostatic correlation, explains the divergence of differential capacitance. They further asserted

that crowding beats overscreening at higher external fields. Since the phenomenological description of the BSK model, efforts have been made to uncover the microscopic mechanism for unconventional EDL features. Démary *et al.* solved 1D lattice Coulomb gas (1D LCG) under the constant voltage ensemble. Their solvable one-dimensional model showed that the 1D LCG undergoes a first-order phase transition between dense and dilute phases by adjusting fugacity [20, 21]. They claimed the transition is closely related to the discontinuous jump in differential capacitance and the transition between camel- and bell-shape capacitance.

Other directions of the approaches use statistical field theory for charged many-body. Earlier mobile point charges with fixed macro-ions were treated within the framework of the statistical field theory of ion systems [15, 22–25]. Recently, Bossa *et al.* adopted the free energy analysis approaches incorporating Yukawa potential to consider the symmetric steric term and successfully reproduced the fourth order potential gradient in BSK equation [26, 27]. They showed that the interplay between short-ranged Yukawa and long-ranged Coulomb interactions can lead to the instability of ILs near an electrode. This instability is characterized by a divergent differential capacitance, indicating a first-order transition [26].

This work uncovers the microscopic origin of the unconventional EDL formation and the consequent phase transition of RTIL capacitance employing a statistical field theory framework. We derive free energy functionals for asymmetric ionic liquids and extracted the modified Poisson equations via saddle point approximation. Our results reveal that the phase transition is triggered by the interplay of the strong electrostatic coupling and the phase demixing due to the asymmetric short-range interaction. We validate our theoretical predictions by comparing them with molecular dynamics simulations. We further elucidate the influence of external electric fields on the phase behavior. This work paves the way for its

* These two authors contributed equally

† ysjho@gnu.ac.kr

‡ wblee@snu.ac.kr

applicability to various systems [28–31].

Statistical Field Theory: We develop a lattice-based model for the electrode of surface charge density σ_e at $x = 0$. The number of the particle at r is $n_{\pm}(r)$ and $\sum_r n_{\pm} = N_{\pm}$. The local densities of each species are $\rho_{\pm}(r) = n_{\pm}(r)/\nu$, where ν is the volume of each lattice. The local charge density is defined as $\rho_c(r) = \rho_+(r) - \rho_-(r)$.

Particles interact with each other through Coulombic and Yukawa interaction:

$$\begin{aligned}\beta u_{+,+} &= \frac{l_B}{r} + a \frac{e^{-\kappa r}}{r} \\ \beta u_{+,-} &= -\frac{l_B}{r} + c \frac{e^{-\kappa r}}{r} \\ \beta u_{-,-} &= \frac{l_B}{r} + b \frac{e^{-\kappa r}}{r},\end{aligned}\quad (1)$$

where l_B is the Bjerrum length, and a, b and c are the Yukawa interaction parameters, and $\beta = \frac{1}{k_B T}$. Then, the total interaction potential energy is represented by

$$\begin{aligned}\beta \mathcal{U}_{tot} &= \frac{1}{2} \int dr dr' \rho_c(r) v_c(r-r') \rho_c(r') \\ &+ \frac{1}{2} \int dr dr' \begin{pmatrix} \rho_+(r) \\ \rho_-(r) \end{pmatrix}^T A_h v_y(r-r') \begin{pmatrix} \rho_+(r) \\ \rho_-(r) \end{pmatrix},\end{aligned}\quad (2)$$

where $A_h = \begin{pmatrix} a & c \\ c & b \end{pmatrix}$, $v_c(r) = l_B/r$, and $v_y(r) = e^{-\kappa r}/r$.

Similarity transformation decouples the Yukawa term with eigenstates.

The grand canonical partition function after the Hubbard-Stratonovich transformation yields,

$$\begin{aligned}\mathcal{Z}_{\lambda} &= \int \mathcal{D}\phi_e \mathcal{D}\phi_1 \mathcal{D}\phi_2 \exp \left(-\frac{1}{8\pi l_B} \int dr (\nabla \phi_e)^2 \right. \\ &- \frac{1}{8\pi \lambda_1} \int dr \left((\nabla \phi_1)^2 + \kappa^2 \phi_1^2 \right) \\ &- \left. \frac{1}{8\pi \lambda_2} \int dr \left((\nabla \phi_2)^2 + \kappa^2 \phi_2^2 \right) \right) \\ &\times \exp \left(\frac{1}{\nu} \int dr \ln (\lambda_s (\mathbf{e}_1 + \mathbf{e}_2)) \right),\end{aligned}\quad (3)$$

where $\mathbf{e}_1 = \exp(-i\phi_e - i\phi_1 \cos \theta + i\phi_2 \sin \theta)$ and $\mathbf{e}_2 = \exp(+i\phi_e - i\phi_1 \sin \theta - i\phi_2 \cos \theta)$. The free energy is,

$$\begin{aligned}\beta \mathcal{F} &= \int dr \left[-\frac{1}{8\pi l_B} (\nabla \psi_e)^2 - \frac{1}{8\pi \lambda_1} \left\{ (\nabla \psi_1)^2 + \kappa^2 \psi_1^2 \right\} \right. \\ &- \left. \frac{1}{8\pi \lambda_2} \left\{ (\nabla \psi_2)^2 + \kappa^2 \psi_2^2 \right\} \right] + \eta(\tilde{\mathbf{e}}_1, \tilde{\mathbf{e}}_2),\end{aligned}\quad (4)$$

where

$$\eta(\tilde{\mathbf{e}}_1, \tilde{\mathbf{e}}_2) = -\frac{1}{\nu} \int dr \ln \{ \lambda_s (\tilde{\mathbf{e}}_1 + \tilde{\mathbf{e}}_2) \},$$

and $\tilde{\mathbf{e}}_1 = \exp(-\psi_e - \psi_1 \cos \theta + \psi_2 \sin \theta)$ and $\tilde{\mathbf{e}}_2 = \exp(+\psi_e - \psi_1 \sin \theta - \psi_2 \cos \theta)$. The saddle-point field approximates the functional integral as,

$$\begin{aligned}\frac{1}{4\pi l_B} \nabla^2 \psi_e &= \frac{1}{\nu} \frac{\tilde{\mathbf{e}}_2 - \tilde{\mathbf{e}}_1}{\tilde{\mathbf{e}}_1 + \tilde{\mathbf{e}}_2} \\ \frac{1}{4\pi \lambda_1} (\nabla^2 - \kappa^2) \psi_1 &= \frac{1}{\nu} \frac{-\cos \theta \tilde{\mathbf{e}}_1 - \sin \theta \tilde{\mathbf{e}}_2}{\tilde{\mathbf{e}}_1 + \tilde{\mathbf{e}}_2}\end{aligned}\quad (5)$$

$$\frac{1}{4\pi \lambda_2} (\nabla^2 - \kappa^2) \psi_2 = \frac{1}{\nu} \frac{\sin \theta \tilde{\mathbf{e}}_1 - \cos \theta \tilde{\mathbf{e}}_2}{\tilde{\mathbf{e}}_1 + \tilde{\mathbf{e}}_2}.$$

When the short-range interaction is symmetric, *i.e.* $a = b$, Eq. 5 yields,

$$\begin{aligned}\frac{\nu}{4\pi l_B} \nabla^2 \psi_e &= \tanh(\psi_e + \psi_h) \\ \frac{\nu}{2\pi(c-a)} (\nabla^2 - \kappa^2) \psi_h &= \tanh(\psi_e + \psi_h),\end{aligned}\quad (6)$$

where $\psi_h = -\psi_2/\sqrt{2}$. For this special case, our Eq. 6 is identical to the equations in previous work [26]. To check correspondences, we used boundary conditions [26, 32]

$$\psi'_e(0) = -\lambda s_e$$

$$\begin{pmatrix} \psi'_1(0) - \kappa \psi_1(0) \\ \psi'_2(0) - \kappa \psi_2(0) \end{pmatrix} = -4\pi A_h \begin{pmatrix} \sigma_1 \\ \sigma_2 \end{pmatrix},\quad (7)$$

where $\lambda^2 = 4\pi l_B/\nu$ and $s_e = \lambda \sigma_e/e$. We set $\sigma_1 = \sigma_2 = 0$ for the simplicity. The numerical solutions of these non-linear differential equations indeed reproduce the previous results [26] perfectly (Fig. S2).

To capture the behavior of the more realistic systems, we delve into asymmetric cases, $a \neq b$. We scale b and c relative to a , $b = a \times \alpha_b$ and $c = a \times \alpha_c$, respectively. Under the zero charge boundary condition of $\sigma_1 = \sigma_2 = 0$, we explore the influence of α_b by numerically solving Eq. 5. Fig. 1.a reveals a deviation of $s_e(\psi_0)$ from the symmetric solution which transits at $\psi_0 = 0$. The emergence of hysteresis in the $s_e(\psi_0)$ curve coincides with a divergence in the differential capacitance $\tilde{C}_{diff} = \frac{1}{d\psi_0/ds_e}$, which suggests the first-order transition during EDLs formation, consistent with the previous studies [26, 32]. Notably, short-range attractions induce overscreening or crowding, which is rarely observed in pure electrostatic systems.

We next investigate the influence of the cation-anion interaction, α_c . Fig. 1-b) demonstrates that increasing α_c shifts the onset of \tilde{C}_{diff} toward lower α_b . This intriguing trend can be attributed to the enhanced aggregation of like-charged ionic liquids at larger α_c . Stronger cation-anion attraction elevates the energy penalty associated with mixing oppositely charged species. We can get insight considering the effective interaction parameter $\xi = a(1 + \alpha_b - 2\alpha_c)$: as α_c increases, EDL transition becomes feasible even at lower α_b .

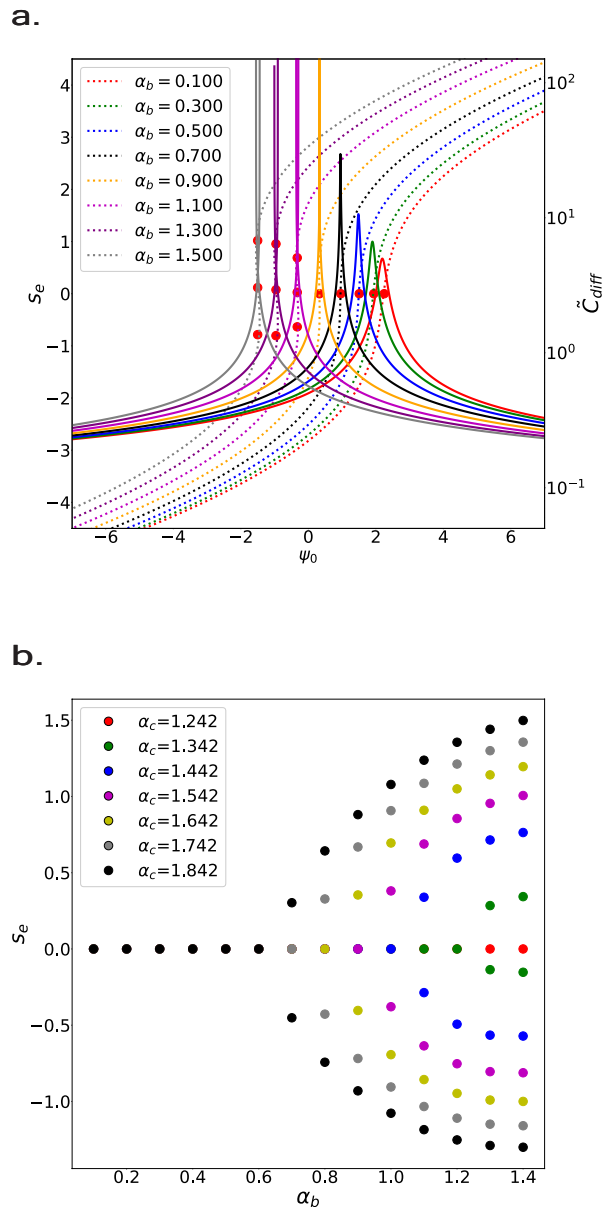


FIG. 1: a) Scaled surface charge density (dotted) and scaled differential capacitance (solid) as a function of surface electrostatic potential by varying α_b values. b) Scaled surface charge density as a function of α_b : α_b varies from 0.1 (most right) to 1.3 (most left) with an increment of 0.2. Red markers indicate s_e at ψ_0 where \tilde{C}_{diff} diverges.

Limiting Case: Some limiting behaviors may provide insights. Setting $a = b$ allows us to recover the BSK equation. If further conditions are imposed on c as $c = a = b$, ψ_h is independent of the electrostatic part and exhibits exponential decay. When $c \gg |a - b|$, $\theta \simeq \pi/4$. Since the Yukawa interaction is only meaningful between oppositely charged ILs, we can remove one of the fields to

obtain a fourth-order differential equation. Conversely, if $c \ll |a - b|$, $\theta \simeq 0$. The Yukawa interactions are decoupled for each sign of charges so that one field is deduced by rewrite 5 in terms of $\psi_e + \psi_1$ and $\psi_e - \psi_2$.

Molecular Dynamics Simulation We perform molecular dynamics (MD) simulations employing Ye's coarse-grained model, which successfully induced the divergence of differential capacitance [33]. We add a Yukawa interaction to Ye's model to compare the simulation results with our theory. The details of the simulation are described in SI.

The local charge density profile, $\rho_c(x) = q(\langle n_+(x) \rangle - \langle n_-(x) \rangle)$, is obtained by averaging simulation configurations. $n_+(x)$ and $n_-(x)$ are the number densities of cations and anions, respectively. The densities are averaged over surface parallel directions. The surface charge density is calculated by,

$$s_e = \frac{\epsilon_r \Delta V}{4\pi L_x} - \frac{1}{L_x} \int_0^{L_x} x \rho_c(x) dx, \quad (8)$$

where ΔV is the difference of constant potential between electrodes [33].

Zero-field simulations ($\Delta V = 0$) show the role of Yukawa potentials in forming EDLs without the charge coupling effects. Fig. 2.a displays that spontaneous surface charge separation (SSCS) is absent until $\alpha_c = 0.9$. It emerges when α_c exceeds 1.0. In addition, the onset of SSCS shifts toward lower values of α_b as α_c increases. This is analogous to our field-theoretic results shown in Fig. 1-b). Notably, despite exploring a reasonable range of Yukawa coefficients, the crowding in EDLs was absent in our zero-field simulations. The parameters in the ref [33] for crowding structure lead to the void formation in our simulation, perhaps due to the Yukawa term. Applying external potentials, the crowding appears across a wide range of the Yukawa coefficients. Fig. 3 shows the crowding emerges above a certain external potential threshold, while overscreening dominates below it.

Previous works, such as ref [19, 34], have identified the external field as a crucial factor governing the transition between overscreening and crowding. Interestingly, our model predicts overscreening, crowding, and bulk phase demixing despite low external fields. The short-range Yukawa interaction plays a critical role in spontaneous surface charge separation and multiple-layer formation inside EDL.

Purely electrostatic systems do not form an electric double layer unless the surface charge density exceeds $1e/nm^2$ or multivalent counter-ions exist. However, ionic liquids exhibit EDL formation even at very low voltages, suggesting an additional driving force beyond simple charge coupling. The multipolar interactions and hardcore repulsion arising from the large, delocalized charges within the ionic liquid induce an alternative way of EDL formation.

Our model captures these non-electrostatic interactions through Yukawa interactions. In the limit that molecules carry zero charges, the effective short-range

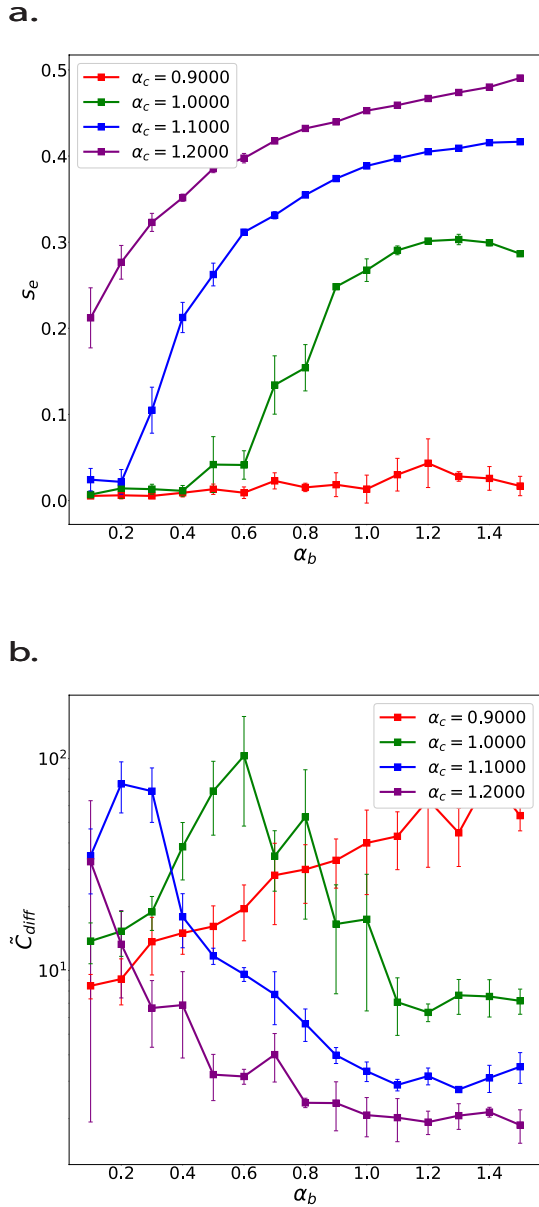


FIG. 2: MD results of charge separation and differential capacitance: a) No spontaneous surface charge separation (SSCS) is observed below $c = 0.9$. Above $c = 1.0$, SSCS occurs, and the onset of SSCS shifts toward smaller α_b consistent with the theory. b) The peak of C_{diff} emerge at the onset of SSCS. Without SSCS, C_{diff} shows no peak.

interaction may be described by $\chi = a(1 + \alpha_b - 2\alpha_c)$. But, in the opposite limit, for example, $\kappa = \infty$, ϕ_1 , and ϕ_2 are zero, the coupling parameter $\Xi = q^2 \frac{l_B}{\mu}$ governs counter-ion condensation. In between, both parameters come into play, influencing the EDL formation.

A negative value of χ leads to spontaneous surface charge separations. At the beginning of the simulation,

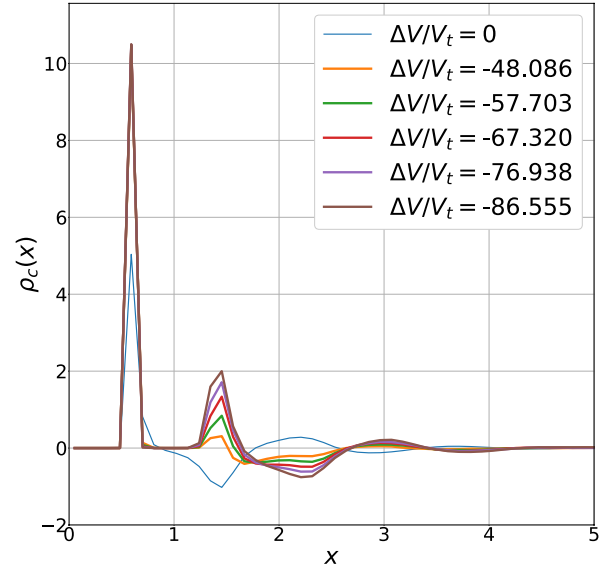


FIG. 3: Charge density profiles varying external field.

two charges form local domains at both electrodes, which may be metastable due to large line tensions [33]. Given enough time, the metastable state transits to a stable state, in which a single charge species is abundant in each electrode [33, 35]. The condensed layer easily overscreens the surface charges, which is extremely difficult to achieve for pure electrostatic cases.

In our case, because the Yukawa coefficients modify the electrostatic interactions also, χ cannot fully explain the surface phase demixing. For instance, increasing a or b has a distinct effect compared to decreasing c , even though both yield the same χ . This is because they also adjust the Coulombic interactions (in other words, the total interaction differs for both cases.). Smaller α_b makes large anionic domain formation difficult, while larger α_c enhances it. If α_c is unreasonably large enough to ignore the Coulomb interaction, it provokes a bulk phase transition of the binary demixing.

Within the parameter range explored in this study, an external field can induce the development of multiple layers of charges, also known as crowding, at the surface (see Fig. 3). While a large surface charge density is required to trigger crowding [36, 37], the onset voltage varies depending on the Yukawa interactions. Stronger short-range repulsion between opposite charges or attraction between like charges reduces the onset voltage Fig. S2. These findings highlight the interplay between the multipolar nature of the ionic liquid (which translates into the strength of the short-range interaction) and the external electric field in determining the overscreening and crowding inside EDL.

The internal structure of EDL at the divergence of \tilde{C}_{diff} is controversial [19]. At the onset of divergence,

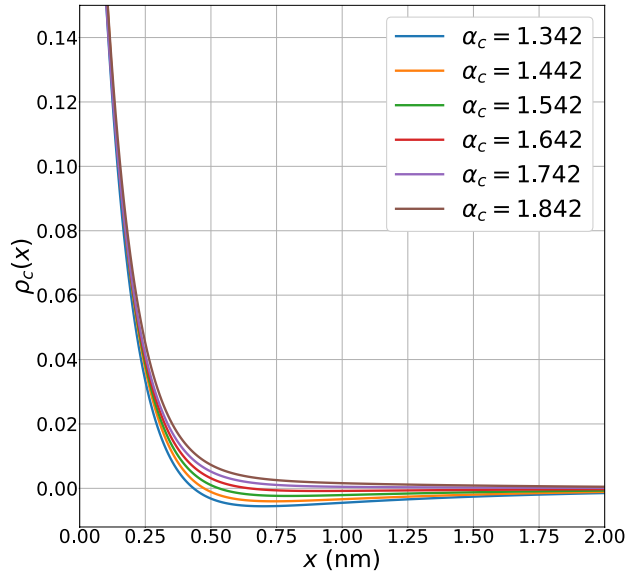


FIG. 4: Local charge density profiles at the onsets of the \tilde{C}_{diff} divergence

our model reveals that the counter-ion arrangement is not determined by a single EDL structure, such as underscreening, overscreening, or crowding. To better understand, we investigate the local charge density profiles at the onset of \tilde{C}_{diff} divergence using our model. The average number of ions is

$$N_{\pm} = \lambda_{\pm} \frac{\partial \ln \mathcal{Z}_{\lambda}}{\partial \lambda_{\pm}}. \quad (9)$$

The local charge density profile is obtained from the loop expansion adopted the zeroth order,

$$\rho_c(r) = \sum_{i=\pm} \frac{N_i}{V} = \left\langle \frac{\tilde{e}_1 - \tilde{e}_2}{\tilde{e}_1 + \tilde{e}_2} \right\rangle = \frac{\bar{e}_1 - \bar{e}_2}{\bar{e}_1 + \bar{e}_2}, \quad (10)$$

where the potential in $\bar{e}_{1,2}$ is used as saddle-point solutions of ψ_e, ψ_1 , and ψ_2 . From the local charge density profiles in Fig. 4, we find that condensed counterions underscreen the surface charge at $c \geq 1.742$. They start to

overscreen the surface charge at $1.342 \leq c \leq 1.642$. It is plausible that large repulsion between different species may induce spontaneous surface charge separation even at low surface charge densities and, hence, below the overscreening condition.

This study delves into the intricate mechanisms of EDL formation at the surface of ionic liquids. It unveils the delicate interplay between two key interactions, the long-range Coulomb potential and the short-range Yukawa potential. The Yukawa potential arises from IL's large delocalized charges.

The Yukawa potential induces spontaneous surface charge separations (or charge condensation), and the Coulomb force enhances the condensation to develop further overscreening or crowding by reinforcing the strong coupling of counter-ions at the surface. At the onset of the divergence of differential capacitance, SSCS occurs. At this critical point, the external field may increase the condensed charges, but the coions would compensate them immediately.

No unique internal structure of EDLs arises at the onset of divergence of \tilde{C}_{diff} . The strength of short-range ion-ion correlations and surface charge density orchestrate the internal structure of EDLs. Considering these ionic liquids' properties, we can apply these results to real-world problems such as supercapacitors and solid-state electrolyte design.

. AUTHOR CONTRIBUTION

This section is intentionally left empty.

. DATA AVAILABILITY

The authors will provide data on reasonable request.

. ACKNOWLEDGEMENT

This research was supported by the National Research Foundation of Korea(NRF) grant funded by the Korea government(MSIT) 2018M3D1A1058633, and 2021R1A2C1014562.

[1] J. S. Wilkes and M. J. Zaworotko, Air and water stable 1-ethyl-3-methylimidazolium based ionic liquids, *Journal of the Chemical Society, Chemical Communications*, 965 (1992).
 [2] R. D. Rogers and G. A. Voth, Ionic liquids, *Accounts of Chemical Research* **40**, 1077 (2007), doi: 10.1021/ar700221n.
 [3] C. Chiappe and D. Pieraccini, Ionic liquids: solvent properties and organic reactivity, *Journal of Physical Organic*

Chemistry **18**, 275 (2005).
 [4] M. Watanabe, M. L. Thomas, S. Zhang, K. Ueno, T. Yasuda, and K. Dokko, Application of ionic liquids to energy storage and conversion materials and devices, *Chemical Reviews* **117**, 7190 (2017), doi: 10.1021/acs.chemrev.6b00504.
 [5] P. Simon and Y. Gogotsi, Perspectives for electrochemical capacitors and related devices, *Nature Materials* **19**, 1151 (2020).

- [6] M. Armand, F. Endres, D. R. MacFarlane, H. Ohno, and B. Scrosati, Ionic-liquid materials for the electrochemical challenges of the future, *Nature Materials* **8**, 621 (2009).
- [7] I. Osada, H. de Vries, B. Scrosati, and S. Passerini, Ionic-liquid-based polymer electrolytes for battery applications, *Angewandte Chemie International Edition* **55**, 500 (2016).
- [8] E. Pomerantseva, F. Bonaccorso, X. Feng, Y. Cui, and Y. Gogotsi, Energy storage: The future enabled by nanomaterials, *Science* **366**, eaan8285 (2019), doi: 10.1126/science.aan8285.
- [9] X. Chen, R. Paul, and L. Dai, Carbon-based supercapacitors for efficient energy storage, *National Science Review* **4**, 453 (2017).
- [10] L. Miao, Z. Song, D. Zhu, L. Li, L. Gan, and M. Liu, Ionic liquids for supercapacitive energy storage: A mini-review, *Energy & Fuels* **35**, 8443 (2021), doi: 10.1021/acs.energyfuels.1c00321.
- [11] P. R. Bueno, Nanoscale origins of super-capacitance phenomena, *Journal of Power Sources* **414**, 420 (2019).
- [12] T. Sato, G. Masuda, and K. Takagi, Electrochemical properties of novel ionic liquids for electric double layer capacitor applications, *Electrochimica Acta* **49**, 3603 (2004).
- [13] M. A. Gebbie, A. M. Smith, H. A. Dobbs, A. A. Lee, G. G. Warr, X. Banquy, M. Valtiner, M. W. Rutland, J. N. Israelachvili, S. Perkin, and R. Atkin, Long range electrostatic forces in ionic liquids, *Chemical Communications* **53**, 1214 (2017).
- [14] A. Eftekhari, Supercapacitors utilising ionic liquids, *Energy Storage Materials* **9**, 47 (2017).
- [15] R. R. Netz and H. Orland, Beyond poisson-boltzmann: Fluctuation effects and correlation functions, *The European Physical Journal E* **1**, 203 (2000).
- [16] L. Yan, Electrostatic correlations: from plasma to biology, *Reports on Progress in Physics* **65**, 1577 (2002).
- [17] C. D. Santangelo, Computing counterion densities at intermediate coupling, *Physical Review E* **73**, 10.1103/physreve.73.041512 (2006).
- [18] A. Naji, M. Kanduć, J. Forsman, and R. Podgornik, Perspective: Coulomb fluids—weak coupling, strong coupling, in between and beyond, *The Journal of Chemical Physics* **139**, 150901 (2013).
- [19] M. Z. Bazant, B. D. Storey, and A. A. Kornyshev, Double layer in ionic liquids: Overscreening versus crowding, *Physical Review Letters* **106**, 046102 (2011), pRL.
- [20] V. Démery, D. S. Dean, T. C. Hammant, R. R. Horgan, and R. Podgornik, Overscreening in a 1d lattice coulomb gas model of ionic liquids, *Europhysics Letters* **97**, 28004 (2012).
- [21] V. Démery, R. Monsarrat, D. S. Dean, and R. Podgornik, Phase diagram of a bulk 1d lattice coulomb gas, *Europhysics Letters* **113**, 18008 (2016).
- [22] R. D. Coalson and A. Duncan, Systematic ionic screening theory of macroions, *The Journal of Chemical Physics* **97**, 5653 (1992).
- [23] R. D. Coalson, A. M. Walsh, A. Duncan, and N. Ben-Tal, Statistical mechanics of a coulomb gas with finite size particles: A lattice field theory approach, *The Journal of Chemical Physics* **102**, 4584 (1995).
- [24] R. R. Netz and H. Orland, Field theory for charged fluids and colloids, *Europhysics Letters* **45**, 726 (1999).
- [25] I. Borukhov, D. Andelman, and H. Orland, Adsorption of large ions from an electrolyte solution: a modified poisson-boltzmann equation, *Electrochimica Acta* **46**, 221 (2000).
- [26] G. V. Bossa and S. May, Stability of ionic liquid modeled by composite coulomb-yukawa potentials, *Physical Review Research* **2**, 10.1103/PhysRevResearch.2.032040 (2020).
- [27] J. P. De Souza and M. Z. Bazant, Continuum theory of electrostatic correlations at charged surfaces, *The Journal of Physical Chemistry C* **124**, 11414 (2020).
- [28] Y. A. Budkov, A. L. Kolesnikov, and M. G. Kiselev, A modified poisson-boltzmann theory: Effects of co-solvent polarizability, *EPL (Europhysics Letters)* **111**, 10.1209/0295-5075/111/28002 (2015).
- [29] R. R. Netz, Electrostatics of counter-ions at and between planar charged walls: From poisson-boltzmann to the strong-coupling theory, *The European Physical Journal E* **5**, 557 (2001).
- [30] A. Levy, D. Andelman, and H. Orland, Dipolar poisson-boltzmann approach to ionic solutions: a mean field and loop expansion analysis, *J Chem Phys* **139**, 164909 (2013), levy, Amir Andelman, David Orland, Henri eng Research Support, Non-U.S. Gov't 2013/11/05 J Chem Phys. 2013 Oct 28;139(16):164909. doi: 10.1063/1.4826103.
- [31] P. Koehl, M. Delarue, and H. Orland, Simultaneous identification of multiple binding sites in proteins: A statistical mechanics approach, *J Phys Chem B* **125**, 5052 (2021), koehl, Patrice Delarue, Marc Orland, Henri eng Research Support, Non-U.S. Gov't 2021/05/12 J Phys Chem B. 2021 May 20;125(19):5052-5067. doi: 10.1021/acs.jpcc.1c02658. Epub 2021 May 11.
- [32] Y. Avni, R. M. Adar, and D. Andelman, Charge oscillations in ionic liquids: A microscopic cluster model, *Phys Rev E* **101**, 010601 (2020), avni, Yael Adar, Ram M Andelman, David eng 2020/02/20 Phys Rev E. 2020 Jan;101(1-1):010601. doi: 10.1103/PhysRevE.101.010601.
- [33] B. B. Ye and Z. G. Wang, A coarse-grained model of room-temperature ionic liquids between metal electrodes: a molecular dynamics study, *Phys Chem Chem Phys* **24**, 11573 (2022), ye, Benjamin Bobin Wang, Zhen-Gang eng England 2022/05/07 Phys Chem Chem Phys. 2022 May 18;24(19):11573-11584. doi: 10.1039/d2cp00166g.
- [34] M. V. Fedorov and A. A. Kornyshev, Towards understanding the structure and capacitance of electrical double layer in ionic liquids, *Electrochimica Acta* **53**, 6835 (2008), eXPLORING FRONTIERS OF ELECTROCHEMISTRY Selection of papers from the 58th Annual Meeting of the International Society of Electrochemistry 10-14 September 2007, Banff, Canada.
- [35] R. Atkin, S. Z. El Abedin, R. Hayes, L. H. S. Gasparotto, N. Borisenko, and F. Endres, Afm and stm studies on the surface interaction of [bmp]tfsa and [emim]tfsa ionic liquids with au(111), *The Journal of Physical Chemistry C* **113**, 13266 (2009), doi: 10.1021/jp9026755.
- [36] A. A. Kornyshev, Double-layer in ionic liquids: Paradigm change?, *The Journal of Physical Chemistry B* **111**, 5545 (2007), doi: 10.1021/jp067857o.
- [37] X. Wang, M. Salari, D.-e. Jiang, J. Chapman Varela, B. Anasori, D. J. Wesolowski, S. Dai, M. W. Grinstaff, and Y. Gogotsi, Electrode material–ionic liquid coupling for electrochemical energy storage, *Nature Reviews Materials* **5**, 787 (2020).

- [38] S. Plimpton, Fast parallel algorithms for short-range molecular dynamics, *Journal of computational physics* **117**, 1 (1995).
- [39] C. Wakai, A. Oleinikova, M. Ott, and H. Weingärtner, How polar are ionic liquids? determination of the static dielectric constant of an imidazolium-based ionic liquid by microwave dielectric spectroscopy, *The Journal of Physical Chemistry B* **109**, 17028 (2005), doi: 10.1021/jp053946+.
- [40] K. A. Dwelle and A. P. Willard, Constant potential, electrochemically active boundary conditions for electrochemical simulation, *The Journal of Physical Chemistry C* **123**, 24095 (2019), doi: 10.1021/acs.jpcc.9b06635.
- [41] J. Hautman, J. W. Halley, and Y. J. Rhee, Molecular dynamics simulation of water between two ideal classical metal walls, *The Journal of Chemical Physics* **91**, 467 (1989).

. SUPPORTING INFORMATION

A. Reduced Lennard-Jones Units

Distance	$r^* = r/\sigma$	Charge density	$\rho^* = \rho_q \sigma^3 / \sqrt{4\pi\epsilon_0\sigma\epsilon}$
Energy	$U^* = U/\epsilon$	Surface charge density	$\sigma_e^* = \sigma_e \sigma^2 / \sqrt{4\pi\epsilon_0\sigma\epsilon}$
Number density	$\rho^* = \rho\sigma^3$	Electric dipole	$M^* = M/\sigma\sqrt{4\pi\epsilon_0\sigma\epsilon}$
Temperature	$T^* = k_B T/\epsilon$	Electric field	$E^* = E\sigma\sqrt{4\pi\epsilon_0\sigma\epsilon}/\epsilon$
Time	$t^* = t\sqrt{\epsilon/m\sigma^2}$	Voltage	$V^* = V\sqrt{4\pi\epsilon_0\sigma\epsilon}/\epsilon$
Charge	$q^* = q/\sqrt{4\pi\epsilon_0\sigma\epsilon}$	Differential capacitance	$C_d^* = C_d\sigma/4\pi\epsilon_0$

ϵ is an energy scale.

B. Pair Potentials of Molecular Dynamics Simulation

This study uses four potentials: the Coulomb, Yukawa, WCA (Weeks-Chandler-Andersen), and Gaussian potentials. Particle-particle particle-mesh (PPPM) is employed to calculate Coulomb potential. The interactions apply between all charges, regardless of whether they are real or image charges. The potential has the form

$$U_{Coul}(r_{ij}^*) = \frac{q_i^* q_j^*}{\epsilon_r r_{ij}^*}, \quad (S1)$$

where q_i^* and q_j^* are the reduced charges of ions i and j , respectively, ϵ_r is the relative permittivity, and r_{ij}^* is distance between $i - j$ pair in a reduced unit.

The Yukawa potential is

$$U_Y(r_{ij}^*) = \begin{cases} \frac{C_{ij}}{r_{ij}^*} \left(e^{-r_{ij}^*/l_c} - e^{-r_c^*/l_c} \right), & r_{ij}^* \leq r_c^* \\ 0, & r_{ij}^* > r_c^* \end{cases} \quad (S2)$$

where C_{ij} represent the Yukawa coefficients between species of i th particle and j th particle. It is a for anion-anion, b for cation-anion, and c for cation-cation. During the simulations, α , is fixed to 0.75 and b and c are varied as $0.1a \leq b \leq 1.4a$ and $0.9a \leq c \leq 1.2a$. They corresponds to α_b and α_c in theoretical formula. l_c is the inverse decay length of the Yukawa potential set to be the ion size in this work. The cutoff distance is set to $r_c = L_x/2$.

The excluded volume interactions between real ions are accounted for by a mixture of WCA and Gaussian potentials.

$$U_{ex}(r_{ij}^*) = U_{WCA}(r_{ij}^*) + U_{Gauss}(r_{ij}^*). \quad (S3)$$

The WCA potential is

$$U_{WCA}(r_{ij}^*) = \begin{cases} 4\epsilon_{ij} \left[\left(\frac{\sigma_{ij}}{r_{ij}^*} \right)^{12} - \left(\frac{\sigma_{ij}}{r_{ij}^*} \right)^6 \right] + \epsilon_{ij}, & r_{ij}^* \leq 2^{1/6} \\ 0, & r_{ij}^* > 2^{1/6} \end{cases} \quad (S4)$$

where ϵ_{ij} and σ_{ij} are the scaled dispersion energy and size of ions, respectively, which are set to $\epsilon_{ij} = 0.01$ and $\sigma_{ij} = 1$. The shifted Gaussian potential is

$$U_{Gauss}(r_{ij}^*) = \begin{cases} A_{ij} \left(e^{-B_{ij}r_{ij}^{*2}} - e^{-B_{ij}} \right), & r_{ij}^* \leq 1 \\ 0, & r_{ij}^* > 1, \end{cases} \quad (S5)$$

where A_{ij} is interaction energy and B_{ij} is interaction range which are set to $A_{ij} = 1000$ and $B_{ij} = 7$ following Ye's work.

These purely repulsive soft potentials accurately capture the excluded volume interactions of RTILs, preventing an unrealistic liquid-to-solid phase transition that can occur in densely packed simulations with hard spheres.

The WCA potential models the non-electrostatic interaction between ions and the electrode. It differs from the excluded volume interaction with cutoff distance $r_c = 2^{-5/6}$ and parameters $\epsilon_{ij} = 100$ and $\sigma_{ij} = 0.5$. The distance between an ion and the electrode is simply measured along the x -axis.

C. Charge Density Profiles under the External Fields from the Molecular Dynamics Simulation

We calculate charge density profiles from the molecular dynamics simulation at the same c and α_{aa} value. In this parameter range, EDLs is overscreened even in the absence of the external field. It turns to crowding applying external fields. As shown in main text, crowding occurs at low external field as the correlation between co-ions is stronger.

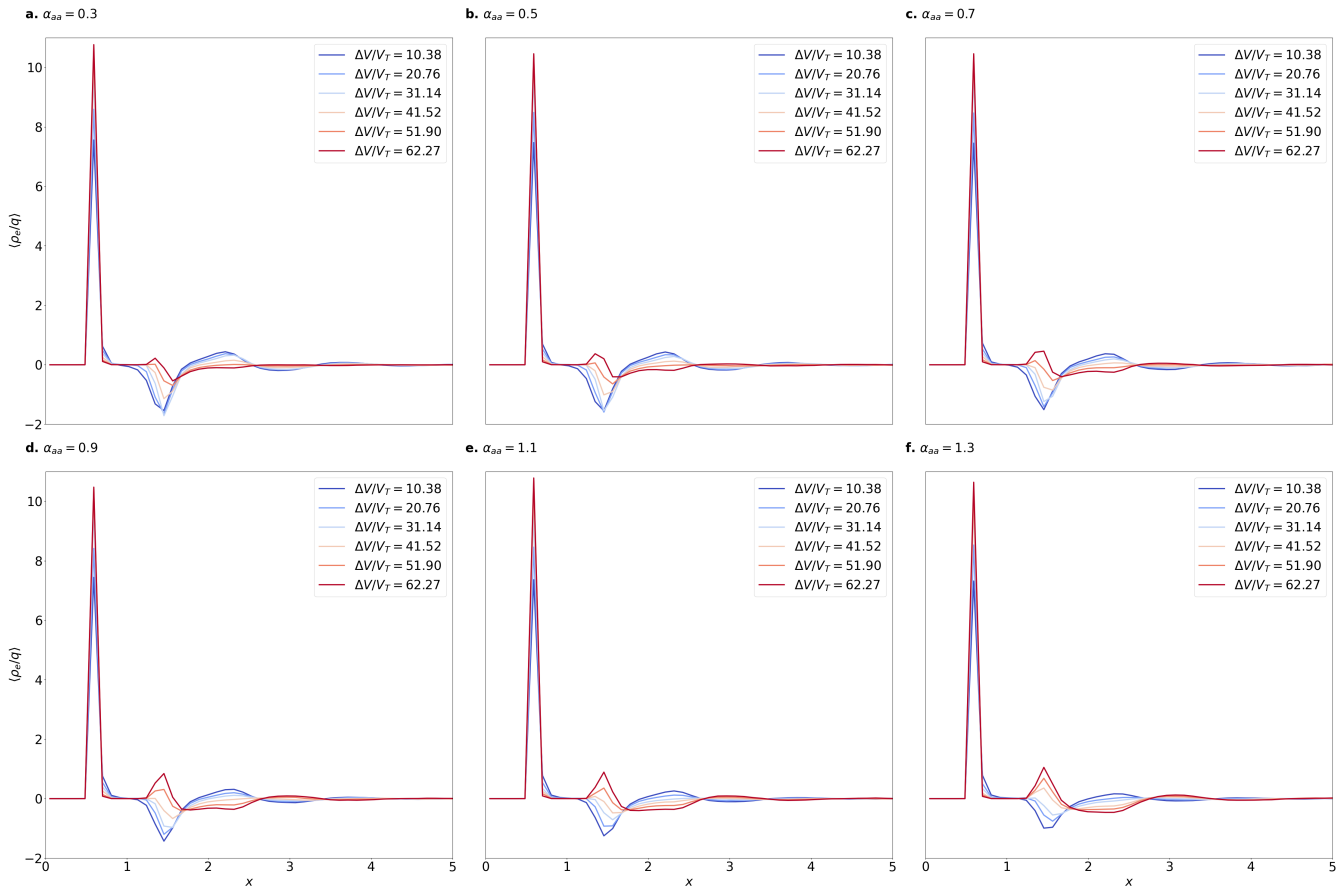


FIG. S1: Charge density profile calculated from simulations applying potential differences with respect to α_{aa}

D. Reproduction of reference data

In Fig. S2, we compare our results with previous report [26, 27]. We find that previous results correspond to a specific case of ours.

E. Crowding Structures

As the BSK model, we find crowding structure if surface charge density is high [19].

F. Statistical Field Theory

We develop a lattice based model for electrode of surface charge density σ_e at $x = 0$. The number of the particle at r is $n_{\pm}(r)$ and $\sum_r n_{\pm} = N_{\pm}$. The local densities of each species are $\rho_{\pm}(r) = n_{\pm}(r)/\nu$, where ν is the volume of each lattice. The local charge density is defined as $\rho_c(r) = \rho_+(r) - \rho_-(r)$.

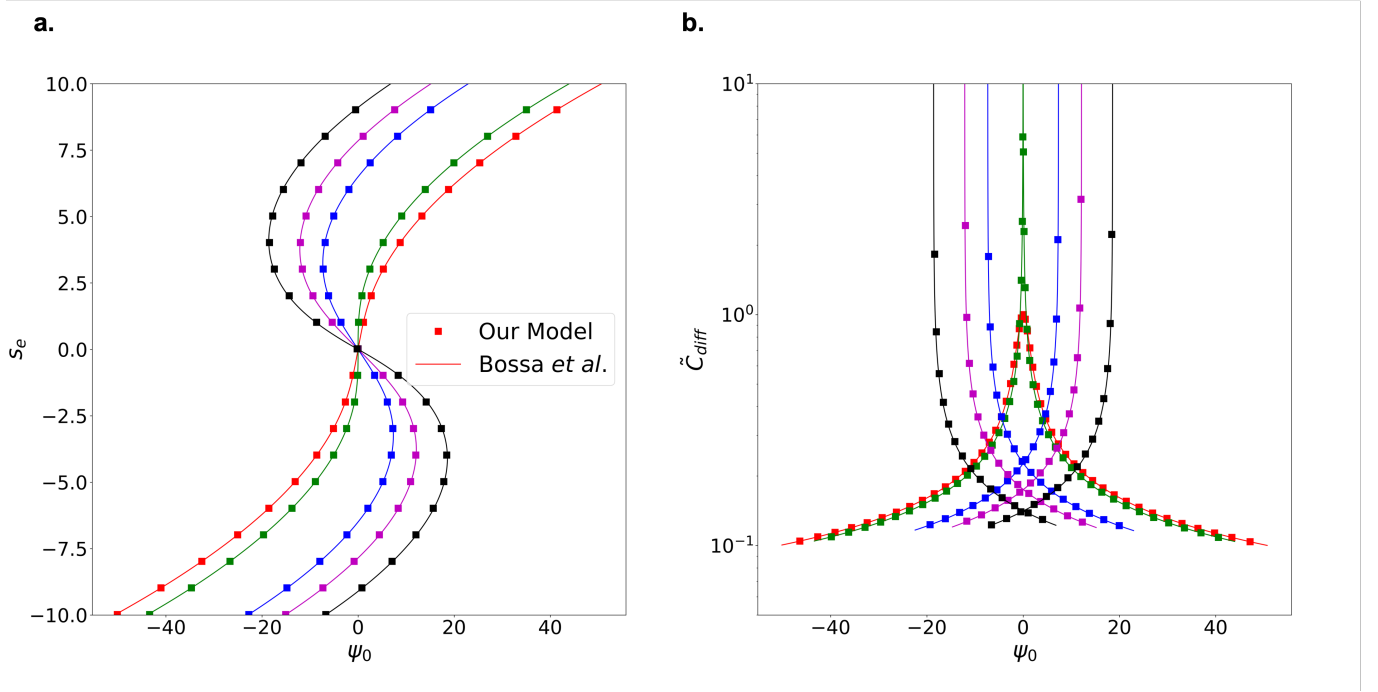


FIG. S2: **a.** Scaled surface charge (s_e) and **b.** differential capacitance (\tilde{C}_{diff}) as a function of surface electrostatic potential ψ_0 , where $\psi_0 = \psi_e(0)$; The results completely matches with the work of Bossa *et al.* in the case of $a = b$. We use $l_B = 8$ nm, $a = b = -2$ nm. $c = -2$ nm (red), $c = 1.342$ nm (green), $c = 10.892$ nm (blue), $c = 14.075$ nm (purple), and $c = 17.258$ nm (black).

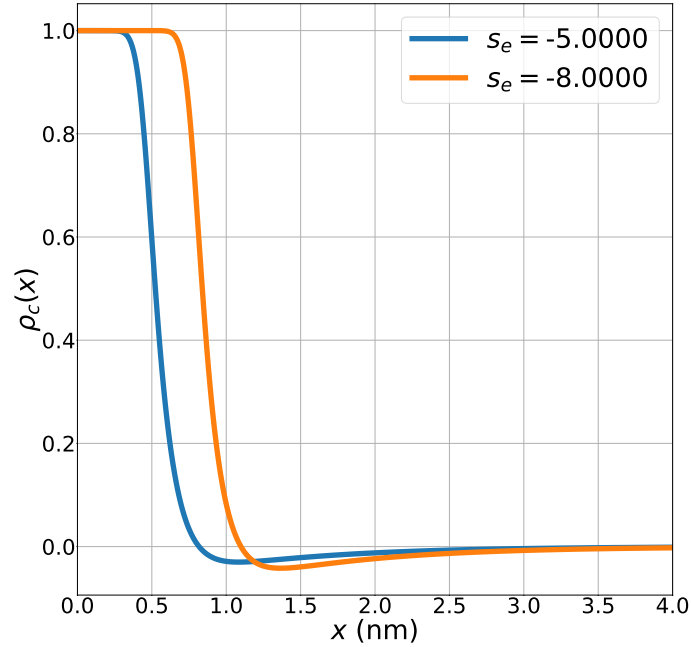


FIG. S3: Local charge density profiles for the strong cation-anion short-range interaction

Particles interact each other through Coulombic and Yukawa interaction:

$$\begin{aligned}\beta u_{+,+} &= \frac{l_B}{r} + a \frac{e^{-\kappa r}}{r} \\ \beta u_{+,-} &= -\frac{l_B}{r} + c \frac{e^{-\kappa r}}{r} \\ \beta u_{-,-} &= \frac{l_B}{r} + b \frac{e^{-\kappa r}}{r},\end{aligned}\tag{S6}$$

where l_B is the Bjerrum length, and a, b and c are the Yukawa interaction parameters, and $\beta = k_B T$. Then, the total interaction potential energy is represented by

$$\begin{aligned}\beta \mathcal{U}_{tot} &= \frac{1}{2} \int dr dr' \rho_c(r) v_c(r-r') \rho_c(r') \\ &+ \frac{1}{2} \int dr dr' \begin{pmatrix} \rho_+(r) \\ \rho_-(r) \end{pmatrix}^T A_h v_y(r-r') \begin{pmatrix} \rho_+(r) \\ \rho_-(r) \end{pmatrix},\end{aligned}\tag{S7}$$

where $A_h = \begin{pmatrix} a & c \\ c & b \end{pmatrix}$, $v_c(r) = l_B/r$, and $v_y(r) = e^{-\kappa r}/r$. Similarity transformation decouples the Yukawa term with eigenstates,

$$\begin{aligned}\beta \mathcal{U}_{tot} &= \frac{1}{2} \int dr dr' \rho_c(r) v_c(r-r') \rho_c(r') \\ &+ \frac{1}{2} \int dr dr' \rho_1(r) v_{y,1}(r-r') \rho_1(r') \\ &+ \frac{1}{2} \int dr dr' \rho_2(r) v_{y,2}(r-r') \rho_2(r'),\end{aligned}\tag{S8}$$

where $v_{y,i}(r) = \lambda_i v_y(r)$ for $i = 1, 2$. The λ_i is

$$\begin{aligned}\lambda_1 &= a \cos^2 \theta + 2c \sin \theta \cos \theta + b \sin^2 \theta \\ \lambda_2 &= a \sin^2 \theta - 2c \sin \theta \cos \theta + b \cos^2 \theta,\end{aligned}$$

and $\rho_i(r)$ is

$$\begin{aligned}\rho_1(r) &= \rho_+(r) \cos \theta + \rho_-(r) \sin \theta \\ \rho_2(r) &= -\rho_+(r) \sin \theta + \rho_-(r) \cos \theta.\end{aligned}$$

Here, θ satisfies,

$$\tan 2\theta = \frac{2c}{a-b}.$$

The canonical partition function of the system is,

$$\begin{aligned}\mathcal{Z}_c &= \sum_{\{n_{\pm}(r)\}} \delta \left(\sum_r n_+(r) - N_+ \right) \delta \left(\sum_r n_-(r) - N_- \right) e^{-\mathcal{U}_{tot}} \\ &= \sum_{\{n_{\pm}(r)\}} \delta \left(\sum_r n_+(r) - N_+ \right) \delta \left(\sum_r n_-(r) - N_- \right) \\ &\times \exp \left(-\frac{1}{2} \int dr dr' \rho_c(r) v_c(r-r') \rho_c(r') \right. \\ &\quad -\frac{1}{2} \int dr dr' \rho_1(r) v_{y,1}(r-r') \rho_1(r') \\ &\quad \left. -\frac{1}{2} \int dr dr' \rho_2(r) v_{y,2}(r-r') \rho_2(r') \right).\end{aligned}\tag{S9}$$

It is more practical to deal with the grand canonical ensemble,

$$\mathcal{Z}_\lambda = \sum_{N_+=0}^{\infty} \sum_{N_-=0}^{\infty} \frac{\lambda_+^{N_+} \lambda_-^{N_-}}{N_+! N_-!} \mathcal{Z}_c.$$

where fugacities λ_\pm are function of the chemical potential μ_\pm , $\lambda_\pm = e^{\mu_\pm}$.

The Hubbard-Stratonovich transformations setting $\lambda_\pm = \lambda_s$ for the charge neutrality condition yields,

$$\begin{aligned} \mathcal{Z}_\lambda &= \int \mathcal{D}\phi_e \mathcal{D}\phi_1 \mathcal{D}\phi_2 \exp \left(-\frac{1}{8\pi l_B} \int dr (\nabla\phi_e)^2 \right. \\ &\quad -\frac{1}{8\pi\lambda_1} \int dr \left((\nabla\phi_1)^2 + \kappa^2\phi_1^2 \right) \\ &\quad \left. -\frac{1}{8\pi\lambda_2} \int dr \left((\nabla\phi_2)^2 + \kappa^2\phi_2^2 \right) \right) \\ &\quad \times \exp \left(\frac{1}{\nu} \int dr \ln (\lambda_s (\mathbf{e}_1 + \mathbf{e}_2)) \right), \end{aligned} \quad (\text{S10})$$

where $\mathbf{e}_1 = \exp(-i\phi_e - i\phi_1 \cos\theta + i\phi_2 \sin\theta)$ and $\mathbf{e}_2 = \exp(+i\phi_e - i\phi_1 \sin\theta - i\phi_2 \cos\theta)$. The free energy is,

$$\begin{aligned} \beta\mathcal{F} &= \int dr \left[-\frac{1}{8\pi l_B} (\nabla\psi_e)^2 - \frac{1}{8\pi\lambda_1} \left\{ (\nabla\psi_1)^2 + \kappa^2\psi_1^2 \right\} \right. \\ &\quad \left. -\frac{1}{8\pi\lambda_2} \left\{ (\nabla\psi_2)^2 + \kappa^2\psi_2^2 \right\} \right] + \eta(\tilde{\mathbf{e}}_1, \tilde{\mathbf{e}}_2), \end{aligned} \quad (\text{S11})$$

where

$$\eta(\tilde{\mathbf{e}}_1, \tilde{\mathbf{e}}_2) = -\frac{1}{\nu} \int dr \ln \{ \lambda_s (\tilde{\mathbf{e}}_1 + \tilde{\mathbf{e}}_2) \},$$

and $\tilde{\mathbf{e}}_1 = \exp(-\psi_e - \psi_1 \cos\theta + \psi_2 \sin\theta)$ and $\tilde{\mathbf{e}}_2 = \exp(+\psi_e - \psi_1 \sin\theta - \psi_2 \cos\theta)$. The functional integral is approximated by the saddle-point field,

$$\begin{aligned} \frac{1}{4\pi l_B} \nabla^2 \psi_e &= \frac{1}{\nu} \frac{\tilde{\mathbf{e}}_2 - \tilde{\mathbf{e}}_1}{\tilde{\mathbf{e}}_1 + \tilde{\mathbf{e}}_2} \\ \frac{1}{4\pi\lambda_1} (\nabla^2 - \kappa^2) \psi_1 &= \frac{1}{\nu} \frac{-\cos\theta\tilde{\mathbf{e}}_1 - \sin\theta\tilde{\mathbf{e}}_2}{\tilde{\mathbf{e}}_1 + \tilde{\mathbf{e}}_2} \\ \frac{1}{4\pi\lambda_2} (\nabla^2 - \kappa^2) \psi_2 &= \frac{1}{\nu} \frac{\sin\theta\tilde{\mathbf{e}}_1 - \cos\theta\tilde{\mathbf{e}}_2}{\tilde{\mathbf{e}}_1 + \tilde{\mathbf{e}}_2}. \end{aligned} \quad (\text{S12})$$

G. Molecular Dynamics Simulation

Based on Ye's coarse-grained model, which successfully induced the divergence of differential capacitance [33], Yukawa interaction is added to compare the results with the theory. Cations and anions carry charges at their center. As the reference work claimed, image charge interactions are included to study the divergence of differential capacitance. In addition to the long-range Coulomb interaction, particles interact each other through combined short-ranged pair potentials. All input parameters and output quantities are scaled by fundamental quantities. The main dimensionless physical quantities are provided in section A of Supporting Information. Simulations are performed using the LAMMPS in the canonical ensemble [38]. The system consists of 1000 real particles and 1000 image particles, with a number density of $\rho = 0.8$, and the temperature is set to $T = 1$ using Langevin thermostat. The simulation box is created with the size of $2L \times L \times L$ where the value of L is determined to satisfy the desired number density $\rho = N/V$. Furthermore, wall potentials are applied at $x = 0$ and $x = L$ to represent two smooth planar electrodes. The relative permittivity, ϵ_r , and Bjerrum length, l_B , are set to typical values used for RTIL systems [19, 36, 39], *i.e.*, $\epsilon_r = 12$ and $l_B = 10$. Moreover, the elementary charges have reduced magnitudes of $q = \sqrt{\epsilon_r l_B T} \simeq 11$.

Energy minimization and equilibration are performed for each simulation over 10^5 timesteps with a step size $\tau = 0.001$. Another $3 \times 10^6 \tau$ steps are spent for data production. As Ye *et al.* claimed simulation converges to the equilibrium state regardless of the initial configurations [33].

In EDLCs simulations, it is crucial to properly treat the interactions between ions and electrodes. An image charge method is an effective way to embrace the dielectric discontinuity between the electrolyte and the surrounding medium. When the relative permittivity of the bounding material is lower (higher) than that of the electrolyte, ions experience repulsion (attraction) with their images. The image charge method is implemented in LAMMPS by Dwelle and Willard [40]. It is based on the method proposed by Hautman *et al.*, which involves considering infinitely repeating systems of image charges when simulating a three-dimensional system with ions [41]. The simulation system is divided into two subsystems: a real system on the right side ($0 < x < L_x$) and an image system on the left side ($-L_x < x < 0$). The image particles possess charges opposite to those of the real particles in the real system, and they are generated at positions symmetric to the real particles relative to the electrode located at $x = 0$. The whole simulation box is repeated as a unit cell.

The short-range ion-ion correlation is modeled by shifted Yukawa potential. For here the potential has the form

$$\beta U_Y(r_{ij}^*) = \begin{cases} \frac{A}{r_{ij}^*} \left(e^{-r_{ij}^*/l_c} - e^{-r_c^*/l_c} \right), & r_{ij}^* \leq r_c^* \\ 0, & r_{ij}^* > r_c^* \end{cases} \quad (\text{S13})$$

where A represents Yukawa coefficient, which is a for cation-cation, b for anion-anion, and c for cation-anion. l_c is the length of the Yukawa potential.

To investigate the effect of asymmetric Yukawa potential, the correlation strength between cation-cation, a , is fixed to 0.75 and b and c are varied within certain ranges: $0.1a \leq b \leq 1.4a$ and $0.9a \leq c \leq 1.2a$. And the cutoff distance is set to $r_c = L_x/2$. Hereinafter, fractions multiplied by the anion-anion coefficient and the cation-anion coefficient will be referred to as α_b and α_c , respectively. Details of rest of pair potentials are explained in the section B of Supporting Information

Subsequently, simulations with uniform electric field are performed to elucidate the effect of asymmetric Yukawa interaction on the formation of crowding structure. Electric fields with strength $-1 \leq E \leq 1$ are applied to model potential differences with strength $-118 \leq \Delta V/V_T \leq 118$. For here, $V_T = k_B T/e \approx 11$ is the thermal voltage in LJ units and α_c and α_b are fixed to 0.75 and 1.1, while α_b being varied.
